Applied Catalysis B: Environmental 339 (2023) 123099

Contents lists available at ScienceDirect

Applied Catalysis B: Environmental

journal homepage: www.elsevier.com/locate/apcatb

Enhancing methanol selectivity of commercial $Cu/ZnO/Al_2O_3$ catalyst in CO_2 hydrogenation by surface silylation

Xiaojing Cui [a,b], Yequn Liu [c], Wenjun Yan [c], Yanfeng Xue [c], Yangang Mei [b], Jiamei Li [d], Xiaoqing Gao [b], He Zhang [b], Shanhui Zhu [c,*], Yulan Niu [b,*], Tiansheng Deng [c,*]

[a] Collaborative Innovation Center of CO2 Conversion and Utilization, Taiyuan Institute of Technology, 31 Xinlan Road, Taiyuan 030008, PR China
[b] Department of Chemistry and Chemical Engineering, Taiyuan Institute of Technology, 31 Xinlan Road, Taiyuan 030008, PR China
[c] Institute of Coal Chemistry, Chinese Academy of Sciences, 27 South Taoyuan Road, Taiyuan 030001, PR China
[d] School of Chemistry and Chemical Engineering, North University of China, Taiyuan 030051, PR China

ARTICLE INFO

Keywords:
CO_2 hydrogenation
Methanol
Commercial $Cu/ZnO/Al_2O_3$ catalyst
Surface silylation
Selectivity

ABSTRACT

Suppressing reverse water-gas-shift (RWGS) reaction is high desirable but challenging and underdeveloped for Cu/ZnO catalysts, particularly for commercial $Cu/ZnO/Al_2O_3$ catalysts. Different from the current methodologies to reduce RWGS reaction, we report a simply surface silylation method for efficiently minimizing RWGS reaction over a commercial $Cu/ZnO/Al_2O_3$ catalyst. This method suppresses STY_{CO} (Space-time yield) from 97.4 to 0.7 $g_{CO}{\cdot}kg_{cat}^{-1}{\cdot}h^{-1}$, improving STY_{MeOH} from 20.2 to 39.9 $g_{MeOH}{\cdot}kg_{cat}^{-1}{\cdot}h^{-1}$ and methanol selectivity from 15.1 to 92.9 mol%. The combination of characterization methods and density functional theory calculations provide insight into the suppressing mechanism of surface silylation on catalyst. A hydroxyl (on ZnO)-promoted RWGS reaction cycle is discovered, which can be efficiently inhibited by the consuming of hydroxyls via surface silyation. Our results provide a way to regulate RWGS reaction on Cu/ZnO-based catalysts and are expected to the further use of silylation strategy to tune the interconversion of CO and CO_2 via RWGS/WGS reaction on hydrogenation catalysts.

1. Introduction

The ability to convert CO_2, an end product in the utilization of carbon resources, into platform molecules and value-added chemicals is important, not only for reducing CO_2 emission and alleviating the environmental problems, but also for establishing the sustainable society [1–8]. CO_2 can transform into C1 platforms such as methanol (CH_3OH), mono oxide (CO) and ethanol, the former of which can be the building block of hydrocarbons and aromatics depending on the catalyst design and optimization [9–11]. Hence, it is considered as a promising route to produce CH_3OH by CO_2 hydrogenation.

Striking efforts have been devoted to developing catalysts for selective hydrogenation of CO_2 into CH_3OH, including copper-based [12–15], noble metal supported [16,17] and metal oxide-based systems [10,18]. Among them, copper-based catalysts, particularly $Cu/ZnO/Al_2O_3$ that has been successfully applied in the commercial methanol production from CO_2-containing syngas ($CO/CO/H_2$), have been extensively exploited [19,20]. Intrigued by their high activity and selectivity in syngas-to-methanol reaction, scientists explored the performances of $Cu/ZnO/Al_2O_3$ in CO_2 hydrogenation to methanol [21–27]. Although $Cu/ZnO/Al_2O_3$ enables hydrogenation of CO_2 to CH_3OH with high activity, it can readily convert CO_2 to CO due to its ability to catalyze RWGS reaction ($CO_2 + H_2 \leftrightarrow CO + H_2O$), resulting in undesired high CO selectivity commonly in the range of 30–80 mol% [20–25].

The reported methods to suppress RWGS reaction and CO selectivity on $Cu/ZnO/Al_2O_3$ include the tuning of preparation processing parameters and addition of promoter(s), in order to increase the dispersion of Cu and its synergy with ZnO, and/or number of surface basic sites [21–28]. Lee et al. demonstrated that for the co-precipitated $Cu/ZnO/Al_2O_3$ catalyst, the clean removal of residual sodium during the washing process improved CH_3OH selectivity from 15.4% to 66.0% at 210 °C and 3 MPa [21]. Deng and co-workers reported an oxalate gel co-precipitation method for the fabrication of ultrafine $Cu/ZnO/Al_2O_3$ catalyst, on which the maximal CH_3OH selectivity reached 53.3% with CO_2 conversion of 14.7% at 220 °C and 2 MPa [22,23]. Fan's group developed a similar gel preparation method to prepare meso- and macroporous $Cu/ZnO/Al_2O_3$ using gelatin polymer, which showed the

* Corresponding authors.
E-mail addresses: zhushanhui@sxicc.ac.cn (S. Zhu), niuyulan@163.com (Y. Niu), dts117@sxicc.ac.cn (T. Deng).

https://doi.org/10.1016/j.apcatb.2023.123099
Received 25 April 2023; Received in revised form 3 July 2023; Accepted 14 July 2023
Available online 22 July 2023

highest CH_3OH selectivity of 32.4% with CO_2 conversion of 17.3% at 240 °C and 2 MPa [24]. Hong and Tsang's team demonstrated a tuning effect of ZnO shape on the selectivity of $Cu/ZnO/Al_2O_3$, and the highest CH_3OH selectivity of 72.9% was achieved at CO_2 conversion of 10.9% on the catalyst with plate-like ZnO at 270 °C and 4.5 MPa [25]. More recently, Dasireddy et al. prepared $Cu/ZnO/Al_2O_3$ catalyst by an ultrasound-assisted co-precipitation method, where CH_3OH selectivity was improved from ca. 50% to ca. 68% at CO_2 conversion of ca. 5% (200 °C and 2 MPa) [26].

In the case of promoter(s), ZrO_2 is an effective one for $Cu/ZnO/Al_2O_3$, which can promote efficiently CH_3OH selectivity [27,28]. Wang et al. found an enhancement of CH_3OH selectivity from ca. 60% to ca. 80% over $Cu/ZnO/Al_2O_3$ at 240 °C and 5 MPa with the addition of ZrO_2 [27]. Besides ZrO_2, addition of the other promoters was reported for $Cu/ZnO/Al_2O_3$, including yttrium (Y) [29] and N-doped graphene (NG) [30]. Sun et al. observed that CH_3OH selectivity of $Cu/ZnO/Al_2O_3$ increased from ca. 58.1% to ca. 70.5% at 230 °C and 5 MPa with addition of Y_2O_3 [29]. Recently, the $Cu/ZnO/Al_2O_3$ catalysts with novel structures were fabricated using different synthetic strategies to improve CH_3OH selectivity [31–34]. A bimetallic metal organic framework (MOF)-templated strategy was developed to synthesize $Cu\text{-}ZnO/Al_2O_3$, which showed high CH_3OH selectivity of 86.9% at CO_2 conversion of 9.1% (240 °C and 3 MPa) [31]. A bifunctional catalytic membrane reactor (CMR) with a $Cu\text{-}ZnO\text{-}Al_2O_3$ layer deposited on a zeolite LTA membrane was synthesized, on which 100% selectivity to CH_3OH was obtained [32].

Compared with the breakthroughs made on the $Cu/ZnO/Al_2O_3$ catalysts prepared in laboratory, the efforts on improving CH_3OH selectivity of commercial $Cu/ZnO/Al_2O_3$ catalysts are few and scarce [35,36]. Ruland et al. reported that CH_3OH selectivity of an industrial $Cu/ZnO/Al_2O_3$ can be tuned from 28.0% to 54.0% by varying reaction conditions [35]. For industrial $Cu/ZnO/Al_2O_3$, it is high desirable to improve CH_3OH selectivity through a simple catalyst treatment, which will benefit methanol yield and also minimize the separation needs. Here we demonstrated that CH_3OH selectivity of a commercial $Cu/ZnO/Al_2O_3$ catalyst can be substantially enhanced from 15.3 mol% to more than 90.0 mol% by a simply surface silylation treatment. The combination of characterization and DFT calculation results show that the hydroxyls on the ZnO surface (i.e., Zn-OHs) participate in RWGS reaction and contribute to CO formation. The surface silylation modification consumed efficiently the Zn-OHs, which suppressed CO formation and highlighted CH_3OH selectivity on the catalyst.

2. Experimental

2.1. Materials

The commercial $Cu/ZnO/Al_2O_3$ (designated as CZA) for methanol synthesis was detailed elsewhere, in which the Cu, Zn and Al contents were 46.2, 19.5 and 4.8 wt%, respectively [33]. Hexamethyl disiloxane (S1: HMSO, 99%), methoxytrimethylsilane (S3: MTMS, 97%), triethoxymethylsilane (S4: TEMS, 98%) and (3-Aminopropyl)triethoxysilane (N1: AEOS, 99%) were purchased from Shanghai Macklin Biochemical Co., Ltd. Tetraethyl orthosilicate (S2:TEOS, AR), toluene (AR) and Fe $(NO_3)_3{\cdot}9\ H_2O$ (AR) were purchased from Sinopharm chemical reagent Co., Ltd (China). 3-glycidyloxypropyl(dimethoxy)methylsilane (S5: GPMS, ≥96.0%(GC)) was purchased from Shanghai Aladdin Biochemical Technology Co., Ltd.

2.2. Preparation of silylated $Cu/ZnO/Al_2O_3$ catalysts

The parameters for the silylation of CZA with single- or bi- silylation reagent(s) were detailed in Table S1 in ESI. For the preparation of S1-CZA-*x* catalysts ($x = 1, 2, 3, 4,$ and 5, respectively), 52.4 g of toluene was mixed with 3.0, 15.0, 30.0, 90.0 g or 180.0 g of hexamethyl disiloxane (HMSO) in a two round-bottomed flask. 3.0 g of CZA catalyst was added, and the whole system was ultrasonicated (40KHz) for 45 min. Then, the whole system was refluxed at 105 °C for 29 h, followed by recovered by centrifugation at 4000 rpm for 5 min, washed with ethanol for 3 times, dried at 100 °C for 12 h, and calcined at 330 °C for 3 h.

The preparation of S2-CZA-*x* catalysts was the same to those of S1-CZA-*x* catalyst, except that the silylation agent was tetraethyl orthosilicate (TEOS) (3.0, 11.5 and 18.9 g of TEOS for S2-CZA-1, 2, and 3, respectively) and the reflux temperature was 115 °C.

The preparation of S3-CZA-*x* catalysts was the same to those of S1-CZA-*x* catalyst, except that the silylation agent was methoxytrimethylsilane (MTMS) (0.84, 3.0, 6.0 and 15.0 g of MTMS for S3-CZA-1, 2, 3 and 4, respectively).

The preparation of S4-CZA-*x* catalysts was the same to those of S1-CZA-*x* catalyst, except that the silylation agent was triethoxymethylsilane (TEMS) (1.5, 3.0, 9.75 and 16.5 g of TEMS for S4-CZA-1, 2, 3 and 4, respectively).

The preparation of S5-CZA-*x* catalysts was the same to those of S1-CZA-*x* catalyst, except that the silylation agent was 3-glycidyloxypropyl (dimethoxy)methylsilane (GPMS) (3.0, 9.0 and 72.9 g of GPMS for S5-CZA-1, 2 and 3, respectively).

The preparation of N1-CZA-*x* catalysts were the same to those of S1-CZA-*x* catalyst, except that the silylation agent was (3-aminopropyl) triethoxysilane (AEOS) (3.0 and 15.0 g of AEOS for N1-CZA-1 and 2, respectively).

A two-step silylation process was carried out for preparing S1-S2-CZA-*x* catalysts ($x = 1, 2, 3, 4, 5,$ and 6, respectively). Initially, 52.4 g of toluene was mixed with 30.0, 30.0, 30.0, 60.0, 99.0 g or 140.0 g of HMSO in a two round-bottomed flask. 3.0 g of CZA catalyst was added, and the whole system was ultrasonicated (40KHz) for 45 min. Then, the whole system was refluxed at 105 °C for 29 h, followed by recovered by centrifugation at 4000 rpm for 5 min, washed with ethanol for 3 times, dried at 100 °C for 12 h. The dried samples were silylated for the second time as following: 52.4 g of toluene was mixed with 3.0, 18.9, 30.0, 30.0, 50.0 g or 80.0 g of TEOS in a two round-bottomed flask, followed by the addition of 3.0 g of dried sample. The whole system was ultrasonicated (40KHz) for 45 min, refluxed at 115 °C for 29 h, followed by recovered by centrifugation at 4000 rpm for 5 min, washed with ethanol for 3 times, dried at 100 °C for 12 h, and calcined at 330 °C for 3 h.

2.3. Catalyst testing

The CO_2 hydrogenation performances for the catalysts were conducted in a continuous-flow fixed-bed reactor equipped with a stainless-steel tube reactor. 0.72 g of catalyst granules (20–40mesh) were mixed with quartz granules of same mesh and then loaded at the same isothermal section of the reactor. Prior to the reaction, all of the catalysts were reduced in situ by a stream of 5.6% H_2/Ar (v/v) under atmospheric pressure at 250 °C for 10 h with a space velocity of 6.0 NL/g-cat/h (CZA and S1-S2-CZA-*5* were also reduced at 360 °C for 10 h to explore the effect of silylation on the thermal stability of catalyst). After the reduction, the reactor was cooled down to 180 °C. The system was pressurized with the reaction gas of H_2/CO_2 ($H_2/CO_2 = 5$, v/v) up to 4.3 MPa. The temperature was gradually increased to 210 °C. The CO_2 hydrogenation reaction was carried out in a flow of the reaction H_2/CO_2 gas at 210 °C with the space velocity of 2.0 NL/g-cat/h, respectively. The gas and liquid products were separated with a cold trap. Both the purified feed gases and the tail gas were analyzed by an online gas chromatograph (GC, GC-4000A, East & West Analytical Instruments (EWAI), Inc.) equipped with a TCD and two flame ionization detectors (FID). H_2, CO_2, and CO were monitored by the TCD with a 5 A mole sieve column, while oxygenates (CH_3OH, and CH_3OCH_3) and CH_4 were detected by the FID with a DB-WAX column (Agilent, 60 m × 0.32 mm × 0.50 μm) and the FID with a HP-PLOT Al_2O_3 KCI column (Agilent, 50 m × 0.32 mm × 8.0 μm), respectively. The liquid aqueous products were analyzed by an EWAI GC (GC-4000A) equipped with a FID with a capillary column (Agilent, 19091 N-136). The CO_2 conversion (designated as X_{CO2}) and

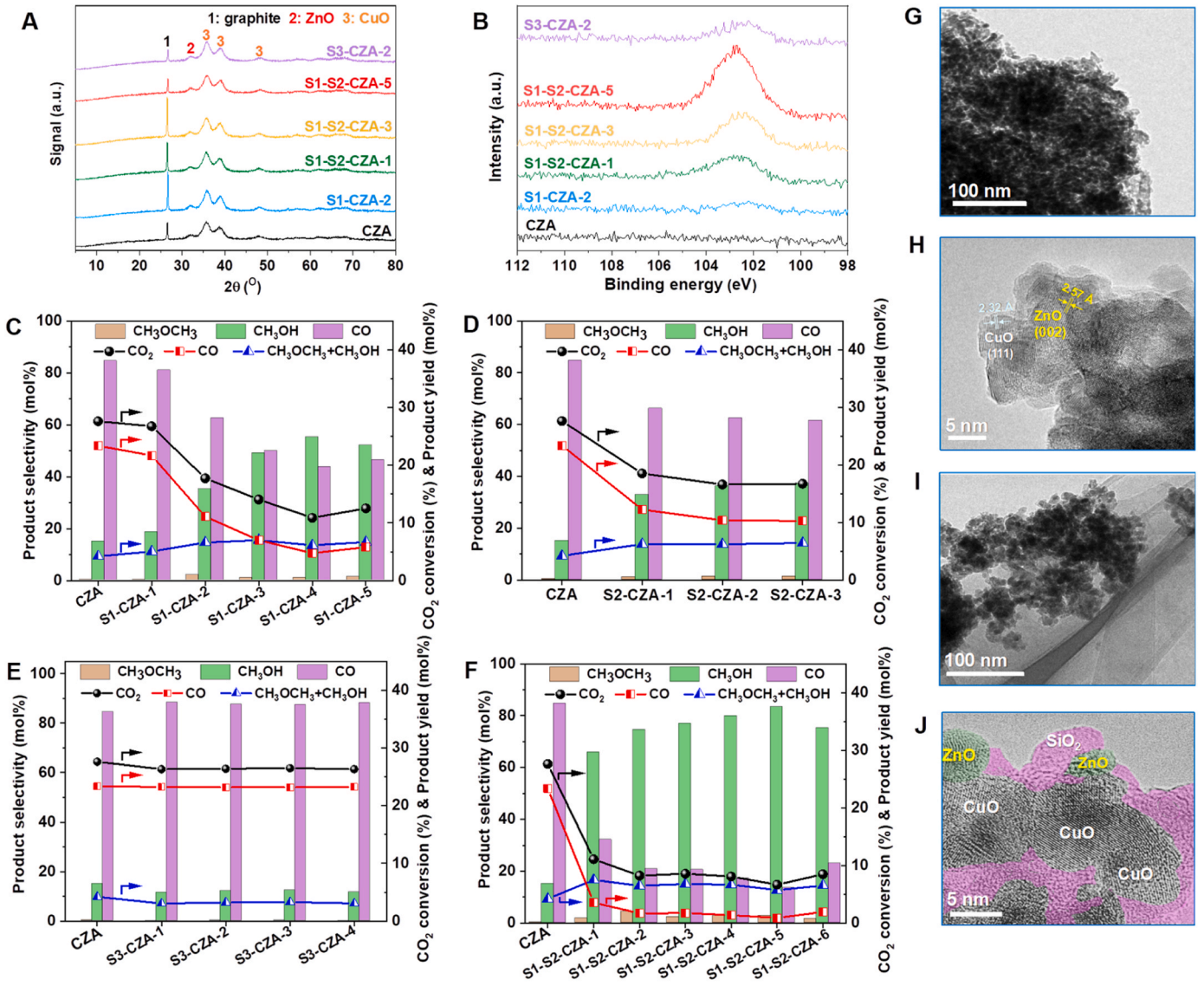

Fig. 1. Analysis of calcined catalysts and their performance for CO_2 hydrogenation to methanol: (A) XRD patterns, (B) Si 2*p* XPS spectra. Performance of: (C) CZA and S1-CZA-*x* catalysts, (D) S2-CZA-*x* catalysts, (E) S3-CZA-*x* catalysts, and (F) S1-S2-CZA-*x* catalysts. HRTEM images of (G-H) calcined CZA catalyst and (I-J) calcined S1-S2-CZA-*5* catalyst (The amorphous SiO_2 in image J was colored with pink).

the carbon-based selectivity of CH_3OH, CH_3OCH_3 (DME), and CO (assigned to S_M, S_{DME} and S_{CO}, respectively) were calculated by an internal normalization method.

The yields of CH_3OH and DME on each catalyst were combined together and referred to as Y_{D+M}. Both Y_{D+M} and Y_{CO} (CO yield) were defined as following:

$$Y_{D+M} = X_{CO2} \times (S_{DME}+S_M);\ Y_{CO} = X_{CO2} \times S_{CO}.$$

2.4. Catalyst characterization

The powder X-ray diffraction (XRD) patterns in the 2θ range from 5 ° to 80 ° were recorded on a Rigaku Miniflex II diffractometer with Cu-Kα radiation source at a scanning rate of 4 °/min.

The transmission electron microscopy (TEM) images, high-resolution TEM (HRTEM) images and elemental distributions of Cu/ZnO/Al_2O_3 (CZA) and silylated CZA catalysts were measured on a JEOL JEM-2100 F microscope operating at 200 k*V*. Before the measurement, the samples were prepared by ultrasonic dispersion for 15 min with ethanol and supported on a carbon-coated copper grid.

X-ray photoelectron spectroscopy (XPS) and Auger electron spectroscopy (XAES) were measured on an AXIS ULTRA DLD spectrometer with Al-Kα X-ray resource ($h\nu = 1486.6$ e*V*). The signal of contaminated carbon C 1 s at 284.8 e*V* was used as the calibration for binding energy values. For in situ XPS characterization, the samples were reduced at 250 °C for 2 h in 10% H_2/Ar (30 mL/min) before the XPS analysis. The spectra were deconvolved with XPS Peak4.1 software by subtracting the Shirley background and applying the Lorentzian-Gaussian function.

H_2 temperature programmed reduction (H_2-TPR) characterization was performed in a quartz microreactor on an AutoChem II 2920 chemisorption analyzer. In each experiment, 50.0 mg of sample was heated from room temperature to 800 °C at a rate of 10 °C/min, and the consumed H_2 was monitored by a thermal conductivity detector (TCD).

In situ DRIFT spectra in the range of 400–4000 cm^{-1} were collected at a resolution of 4 cm^{-1} on a Nicolet iS10 FTIR spectrometer equipped with a Harrick Praying Mantis™ Low Temperature Chamber and a HiCube 80 Eco vacuum pump. Before the collection, 20 mg of sample was reduced at 250 °C for 2 h in a 10%H_2/Ar flow (30 mL/min). After cooling down to 210 °C in 10%H_2/Ar flow, a (CO_2 +H_2) stream (30 mL/

min, CO_2/H_2 = 5:1, v/v) was in situ introduced into the cell, and the spectra were collected at different reaction times (0–120 min). Then, the sample was cooling down to 40 °C and evacuated at different reaction times (0–10 min, from 1 atm to 10^{-3} Pa). The spectra were collected before and during the evacuation. For S1-S2-CZA-*5* sample, after evacuation at 40 °C for 10 min, the sample was heated to 210 °C, and then evacuated at 210 °C until 30 min, in order to remove the adsorbed surface species on the sample as much as possible. The spectra were collected during the evacuation at 210 °C.

2.5. Density functional theory (DFT) calculation

All calculations were performed with Vienna ab initio simulation package (VASP) code using plane-wave-based periodic DFT method [37]. The exchange and correlations energies were computed by Perdew and Wang (PW91) [38], while the core electrons of elements were treated by spin-polarized generalized gradient approximation and projector augmented wave (PAW) method [39]. The cutoff energy of plane-wave basis was set as 450 eV and the gamma point special k-points sampling were employed. Based on XRD, XPS, TEM and in situ DRIFT results, the Cu/ZnO interface was modeled with a small hydroxylated ZnO clusters ($Zn_6O_7H_7$) bound to Cu (1 1 1) facet [1], in which a 6 × 6 supercell with 3-layer slab was built to describe Cu (1 1 1) facet. On ZnO/Cu (1 1 1) model (Fig. S18 in ESI), the atoms in the bottom layer of Cu (1 1 1) were frozen, while other atoms were allowed to relax during the DFT calculations. A vacuum layer of 15 Å thickness was chosen to eliminate artificial interactions between the slab and its periodic images along the direction perpendicular to ZnO/Cu (1 1 1) slabs. Adsorption energy (E_{ads}) of adsorbate was calculated relative to clean slab (E_{slab}) and substrate gas molecule (E_{sub}). The calculation equation of E_{ads} is described as $E_{ads} = E_{sub/slab} - E_{slab} - E_{sub}$, in which $E_{sub/slab}$ is the total electronic energy of adsorbed substrate on slab model. The transition state (TS) configuration of every elementary reaction step was located by climbing image nudged elastic band (CI-NEB) method [40], and verified by a single imaginary frequency along the reaction coordinate. Activation energy (E_a) was defined as the energy difference between TS and initial state (IS). Reaction energy (E_r) of every elementary reaction was estimated by the energy difference between final state (FS) and TS.

3. Results and discussion

3.1. Tuning effect of surface silylation on catalyst performance

Initially, the surface of commercial $Cu/ZnO/Al_2O_3$ (designated as CZA) was reacted with single reagent to fabricate the silylated CZA catalysts for CO_2 hydrogenation to methanol (Table S1 in ESI). The silylation reagent include hexamethyl disiloxane (S1: HMSO), tetraethyl orthosilicate (S2: TEOS), methoxytrimethylsilane (S3: MTMS), triethoxymethylsilane (S4: TEMS), 3-glycidyloxypropyl(dimethoxy)methylsilane (S5: GPMS), and (3-aminopropyl) triethoxysilane (N1: AEOS) for S1-, S2-, S3-, S4-, S5- and N1-CZA-*x* catalysts, respectively. The surface silylation had little influence in the catalyst structure. As displayed in Fig. 1A, the XRD patterns of silylated catalysts were comparable to that of pristine CZA, all showing the characteristic peaks of CuO, ZnO and graphite with the similar intensity and shape. HRTEM showed the close-packed nanoparticles (NPs) in CZA (Fig. 1G-1H). The Cu and Zn oxides in CZA were CuO and ZnO, showing the lattice spacings of 2.28–2.38 Å (CuO (111) plane) and 2.57–2.67 Å (ZnO (002) plane), respectively (Table S2 in ESI). Different from CZA, the Si signal appeared in the Si 2*p* XPS spectra of silylated catalysts, indicating the successful grafting of silylation reagent molecules on the catalyst surface (Fig. 1B).

The performances for CO_2 hydrogenation to methanol over all of the catalysts were evaluated at 210 °C under 4.3 MPa in a H_2/CO_2 gas (H_2/CO_2 = 5:1, v/v). The main products include CH_3OH, CO and CH_3OCH_3 (DME), which selectivities are designated as S_{CH3OH}, S_{CO} and S_{DME}, respectively. As DME is the dehydration product of CH_3OH, the yields of CH_3OH and DME on each catalyst are combined together and referred to as Y_{D+M}, while that of CO is marked as Y_{CO}. CZA catalyst showed low S_{CH3OH} of 15.1 mol% and high S_{CO} of 84.7 mol% (Fig. 1C, Fig. S1 in ESI), implying the prevalence of reverse water-gas shift (RWGS) reaction. For S1-CZA-*x* catalysts, the increase of HMSO amount from S1-CZA-*1* to S1-CZA-*5* catalyst caused the decrease of Y_{CO} from 23.4 mol% to 4.8 mol% and of S_{CO} from 84.7 mol% to 43.7 mol% (Fig. 1C). This result indicated that CO formation, i.e., RWGS reaction, was suppressed by the surface silylation. The suppression in CO formation resulted in the decreased CO_2 conversion and the improved S_{CH3OH}. The improvement in S_{CH3OH} and decrease in CO_2 conversion compensate each other and made the yield of methanol and DME (Y_{M+D}) almost invariant (Fig. 1C).

The suppression effect of surface silylation on CO formation was also observed over the other silylated CZA catalysts. For S2-CZA-*x* catalysts, Y_{CO} was reduced from 23.4 mol% to a minimum of 10.3 mol%, accompanied by the drop of S_{CO} from 84.7 mol% to 61.4 mol% (Fig. 1D). Compared with S1- and S2- CZA-*x* catalysts, the suppression in CO formation was less obvious over S4-, S5- and N1- CZA-*x* catalysts (Fig. S2 in ESI). The minimal Y_{CO} reached 11.7 mol%, 15.2 mol% and 12.1 mol%, with the lowest S_{CO} of 66.8 mol%, 79.6 mol% and 75.6 mol % over S4-, S5- and N1- CZA-*x* catalysts, respectively. On the contrary, the silylation with MTMS had little impact on the catalyst performance, and the activity and selectivity over S3-CZA-*x* catalysts were similar to those of CZA (Fig. 1E, Fig. S1 in ESI).

Because HMSO and TEOS are more capable of suppressing CO formation than the other silylation reagents, both of them were chosen for the joint silylation of CZA. Briefly, CZA was silylated with HMSO and then with TEOS, and the resulting catalysts were designated as S1-S2-CZA-*x* catalysts, where *x* = 1, 2, 3, 4, 5, and 6, respectively (the larger the *x* value, the higher the amount of HMSO and TEOS during silylation, see Table S1 in ESI). Compared with CZA and the single silylated catalysts, S1-S2-CZA-*x* catalysts had comparable bulky structure (Fig. 1A), but more surface Si species, as indicated by the intensified Si 2p peak in XPS and ICP analysis (Fig. 1B, Table S3 in ESI). After calcination, the surface Si species on the catalyst transformed to amorphous mesoporous SiO_2 layers surrounding CuO and/or ZnO NPs (Fig. 1I-1J).

Surprisingly, the existence of more surface SiO_2 species on S1-S2-CZA-*x* catalysts caused the more obvious suppression of CO formation, compared with the single silylated counterparts (Fig. 1F, Fig. S1 in ESI). The Y_{CO} of S1-S2-CZA-*1* was largely reduced to 3.6 mol%, accompanied by a substantial decline in S_{CO} to 32.1 mol%. As the amount of silylation reagents was further increased, both Y_{CO} and S_{CO} were decreased, reaching the minimum values on S1-S2-CZA-*5*. The Y_{CO} of S1-S2-CZA-*5* was 0.9 mol%, while its S_{CO} reached 13.5 mol%. In contrast, the surface SiO_2 species has much less impact on methanol formation. The Y_{M+D} was comparable over all of the S1-S2-CZA-*x* catalysts.

As CO_2 hydrogenation to methanol is a conversion-selectivity limit reaction, the CH_3OH selectivity will increase with decreasing CO_2 conversion. To rule out the effect of conversion level on the selectivity, the conversion of CZA was tuned via increasing space velocity to the comparable levels to those of the single silylated and combined silylated catalysts, respectively. As shown in Fig. S3 in ESI, the CH_3OH selectivity of CZA reached 16.8 mol% and 35.8 mol% with CO_2 conversion of 18.7% and 9.3%, respectively, which are much lower than those of the silylated counterparts. Thus, it is the surface SiO_2 species that inhibited effectively CO formation, contributing to large enhancement in S_{CH3OH} up to 83.3 mol%.

Commonly, the $Cu/ZnO/Al_2O_3$ catalysts for CO_2 hydrogenation exhibited the CH_3OH selectivity of 12.6–66.0%. The current high-performance Cu/ZnO systems are generally obtained by adding promoter(s) such as ZrO_2 or prepared with a specific structure such as MOF and membrane reactor, showing CH_3OH of 38.4%– 100% (Table S4 in ESI). Different from these studies, a simple surface silylation method can enhance substantially CH_3OH selectivity of $Cu/ZnO/Al_2O_3$ in this work.

Moreover, the typical silylated catalysts including S1-CZA-*2*, S1-S2-CZA-*1*, S1-S2-CZA-*4* and S1-S2-CZA-*5* were chosen, on which the impact

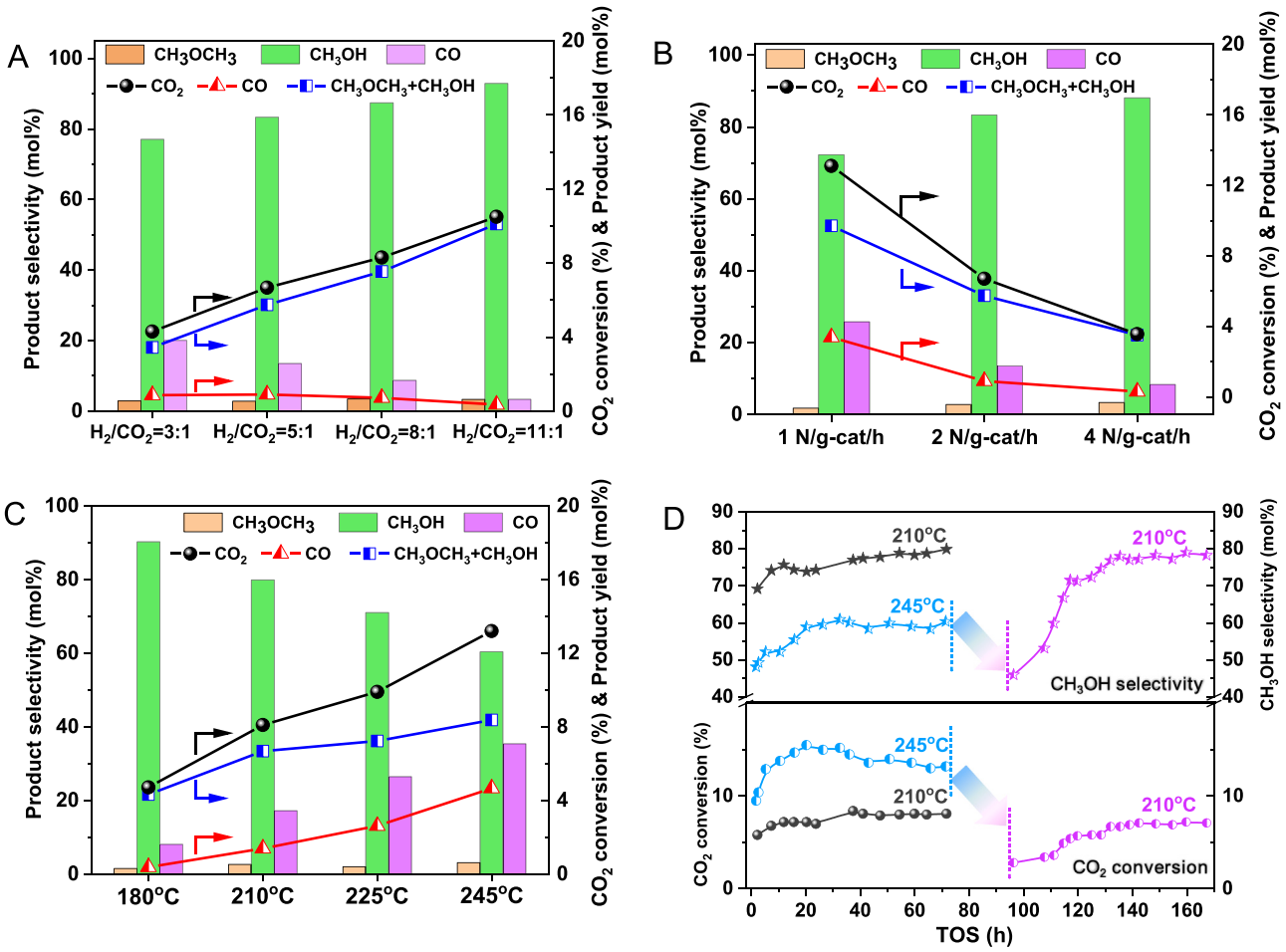

Fig. 2. Impact of reaction conditions on performance for CO_2 hydrogenation to methanol: Influence of (A) H_2/CO_2 volume ratio and (B) space velocity in the performance over S1-S2-CZA-*5*, (C) Effect of reaction temperature on the performance of S1-S2-CZA-*4*, (D) Performance recovery on S1-S2-CZA-*4*: initially reacted at 245 °C for 72 h, and then at 210 °C for another 72 h (a 24 h period for adjusting the temperature: cooled down from 245 °C to room temperature and then raised to 210 °C). For better comparison, the performance of S1-S2-CZA-*4* at 210 °C is included in Fig. 2D. (Conditions: (A): 210 °C, 4.5 MPa, 2 NL/g-cat/h, (B): 210 °C, 4.5 MPa, H_2/CO_2 = 5:1, (C and D): 4.5 MPa, H_2/CO_2 = 5:1, 2 NL/g-cat/h).

of reaction conditions on the performance was explored (Fig. 2, Fig. S4 in ESI). CH_3OH selectivity increased along with the H_2/CO_2 volume ratio or space velocity to the maximum of 92.9 mol% (Fig. 2A-2B). Although the rise of reaction temperature promoted CO_2 conversion, it had a detrimental effect on CH_3OH selectivity (Fig. 2C). The loss of CH_3OH selectivity at high temperatures was not caused by the catalyst deactivation, as the performance of catalyst recovered when the temperature was cooled down to 210 °C (Fig. 2D). High reaction temperatures commonly facilitate RWGS reaction that is an endothermic reaction.

Besides, the stability of S1-S2-CZA-*4* and S1-S2-CZA-*5* catalysts was also explored (Fig. 3). The selectivity and yield of CH_3OH over CZA showed a decrease trend with time-on-stream, while no deactivation was observed over S1-S2-CZA-*4* (Fig. 3A-3B). The silylated catalysts show higher thermal stability than CZA. As shown in Fig. 3C-3D and Fig. S5 in ESI, the rising of reduction temperature from 250 °C to 360 °C had little influence in the performance and the size of active metallic Cu (Cu^0) NPs over S1-S2-CZA-*5*, whereas it caused the decrease of Y_{M+D} on CZA from 4.2 mol% to 2.8 mol%, and also agglomeration of active Cu^0 NPs in the catalyst.

3.2. The location of Si species on the catalyst surface

The SiO_2 species introduced by silylation had an irreplaceable role in regulating CO formation on the catalyst. Hydrophobic SiO_2 NPs was also introduced into CZA by physical mixing to fabricate CZA+SiO_2 catalyst (with a Si content of 2.92 wt% same to that (2.92 wt%) in S1-S2-CZA-*5*, see ICP results in Table S3 in ESI). The performance of CZA+SiO_2 catalyst was comparable to that of CZA (Fig. S6 in ESI). Hence, it is the surface SiO_2 species introduced by silylation that affects the catalyst performance. The surface SiO_2 species suppressed CO_2 hydrogenation to CO, which decreased the overall CO_2 conversion. This decreasing trend of CO_2 conversion over the silylated catalysts is in accordance with their CO_2 and H_2 adsorption amount (Fig. S7-S10, Table S5 in ESI). It is likely that the SiO_2 species covered the surface sites of CZA surface, where CO_2 and H_2 were adsorbed, activated, and then reacted to form CO. Hence, to understand how the surface silylated SiO_2 species suppressed CO formation, it is essential to detail the location of SiO_2 species on the catalyst surface. As the chemistry of surface O will vary with the covered SiO_2 species, the location of SiO_2 species was detected by the O 1*s* XPS analysis. The O 1*s* XPS spectra of the typical silylated catalysts (with large variation in the activity of RWGS reaction, Fig. S1 in ESI) and also CZA were collected and fitted, as shown in Fig. 4A-4B. The spectra of CuO, ZnO and SiO_2 were also recorded for reference, which showed the characteristic peaks at 529.7, 530.2 and 532.1 eV, respectively.

For CZA, the peaks for the O species from CuO and ZnO were present, while the other two peaks centering at 528.1 and 531.9 eV were attributed to the O species in graphite [41] and Al_2O_3 [26], respectively. For S1-CZA-*2* silylated with HMSO, the O contents for CuO and ZnO decreased, accompanied by the increase in the O content for SiO_2. This

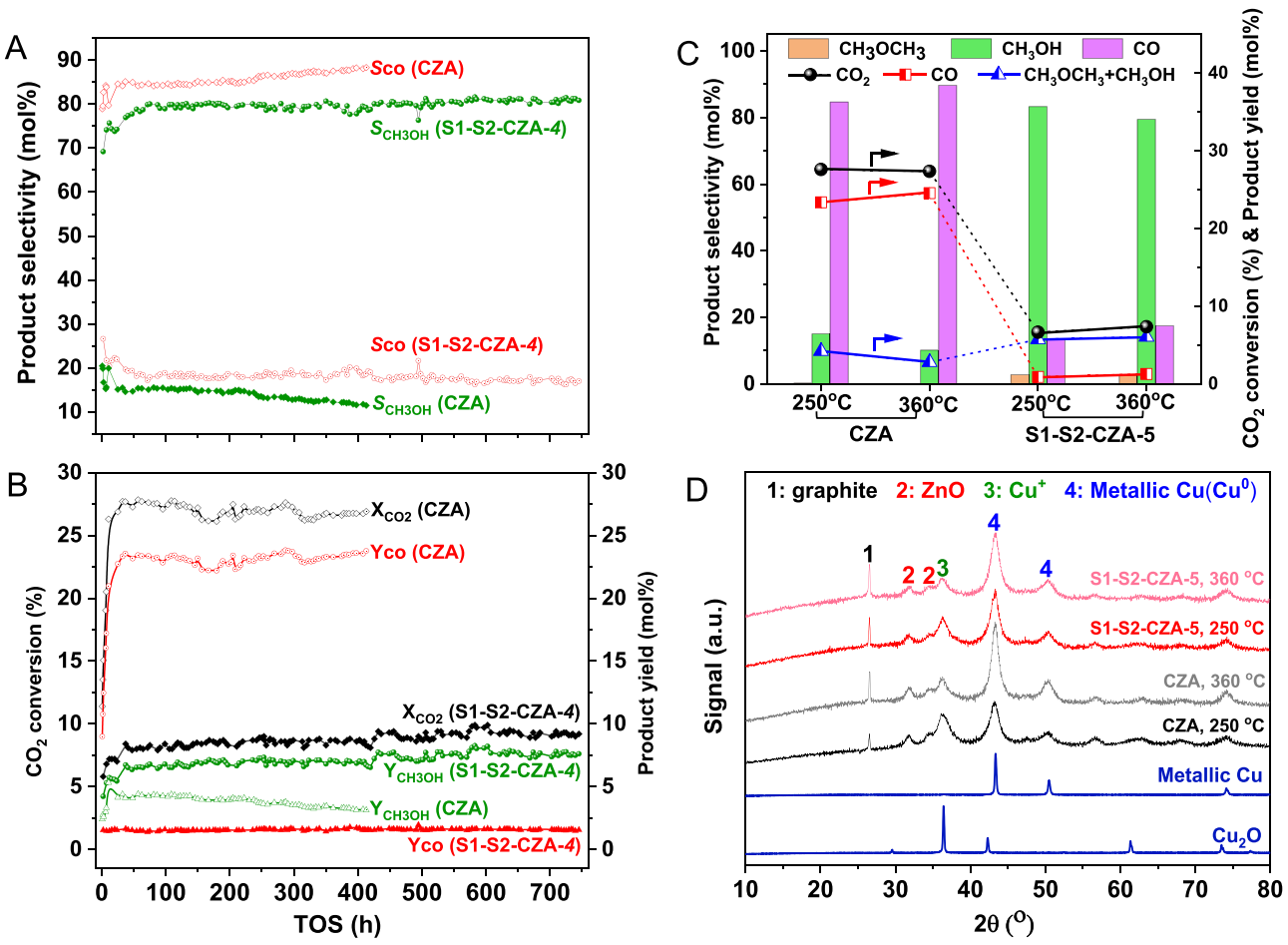

Fig. 3. Stability of silylated catalyst for CO_2 hydrogenation to methanol. Methanol (S_{CH3OH}) and CO (S_{CO}) selectivity (A), and CO_2 conversion (X_{CO2}), methanol yield (Y_{CH3OH}) and CO (Y_{CO}) yield (B) on the long-term catalytic test on CZA and S1-S2-CZA-*4* catalysts; (C) Performance of CZA and S1-CZA-*5* catalysts reduced at 250 °C and 360 °C, respectively, (D) their XRD patterns after reaction for 72 h (Reaction condition in (A-D): 210 °C, 4.5 MPa, and 2 NL/g-cat/h).

result indicated the coverage of SiO_2 species on both the CuO and ZnO surfaces.The coverage of SiO_2 on the CuO and ZnO surfaces was more obvious on S1-S2-CZA-*x* catalysts silylated with HMSO and TEOS, as indicated by the larger decline in the O contents for CuO and ZnO. The coverage of SiO_2 on the CuO and ZnO surfaces was also confirmed by the progressively increase in the O content for SiO_2. Compared with SiO_2, the binding energy (BE) of O 1 s peak of SiO_2 species on the silylated catalysts shifted to a lower value of 531.7 eV. The Si species were grafted on CuO and ZnO surface by reacting with the Cu-OHs and/or Zn-OHs there, forming Cu-O-Si and Zn-O-Si structures. Compared with Si-O-Si structure in silica, the weak Cu-O and Zn-O bonds in Cu-O-Si and Zn-O-Si structures make escape of electron(s) from the Si-O bonds easier, resulting in the lower BEs of O 1 s peak. Particularly, compared with CZA, the O contents for CuO and ZnO over S1-S2-CZA-*5* declined substantially by ca. 93.0% and 91.0%, respectively, indicating coverage of the majority of CuO and ZnO surfaces by the SiO_2 species. Noticeably, the location of SiO_2 species on the surface of S3-CZA-*2* was distinct from the other silylated catalysts. The O content for ZnO was comparable to that of CZA, whereas its O content for CuO was remarkably reduced compared with CZA (Fig. 4A-4B). This result indicated the preferential coverage of SiO_2 species on the CuO surface of S3-CZA-*2*.

Because the silylation was performed on the oxide catalysts, it is possible that the SiO_2 species detached from CuO and/or ZnO surface of catalyst during the reaction. To rule out this possibility, HRTEM and XPS analysis were applied to detect the SiO_2 species on the used catalyst. As shown in Fig. 4C-4G, besides ZnO NPs, Cu^0 and Cu_2O NPs (with the lattice spacings of 1.76–1.86 Å ((200) plane) and 2.10–2.20 Å ((200) plane), respectively) were observed in all of the used catalysts, in accordance with the XRD results (Table S2 and Fig. S11 in ESI). As indicated by HRTEM analysis, SiO_2 species was absent in the used CZA (Fig. 4C and 4H), but presented in the silylated catalysts (Fig. 4D-4H). For the used S1-CZA-*2*, both the surfaces of CuO and ZnO NPs were covered by the SiO_2 species, but the coverage was incomplete with the exposure of naked CuO and ZnO surfaces (Fig. 4E). The abundant SiO_2 species on the used S1-S2-CZA-*x* catalysts made the coverage of CuO and ZnO surfaces more complete (Fig. 4F-4G). In contrast, the SiO_2 species tended to be around the CuO NPs on the used S3-CZA-*2* (Fig. 4D). These results are in accordance with the above O 1 *s* XPS result, indicating the preservation of SiO_2 species on the catalyst surface after reaction.

3.3. *Tuning mechanism of surface Si species on catalyst performance*

To elucidate how the location of surface SiO_2 species regulates the CO formation activity on catalyst, several characterization methods were performed. After the catalytic tests, XRD measurement showed no significant variation in the phase composition and the Cu^0 NPs size for CZA and all of the silylated catalysts (Fig. S11 in ESI). Obviously, the regulating effect of SiO_2 on CO formation did not result from the variation in the bulky structure of catalyst. Cu^0 species are generally considered as the active sites for CO_2 hydrogenation [1,2,21,26,28,29]. The differently distributed SiO_2 species on the surface of catalysts may affect the amount of active Cu^0 species, leading to the difference in CO formation. To exclude this assumption, H_2-TPR and in situ XPS were performed. H_2-TPR showed that the reduction of CuO to Cu^0 shifted to

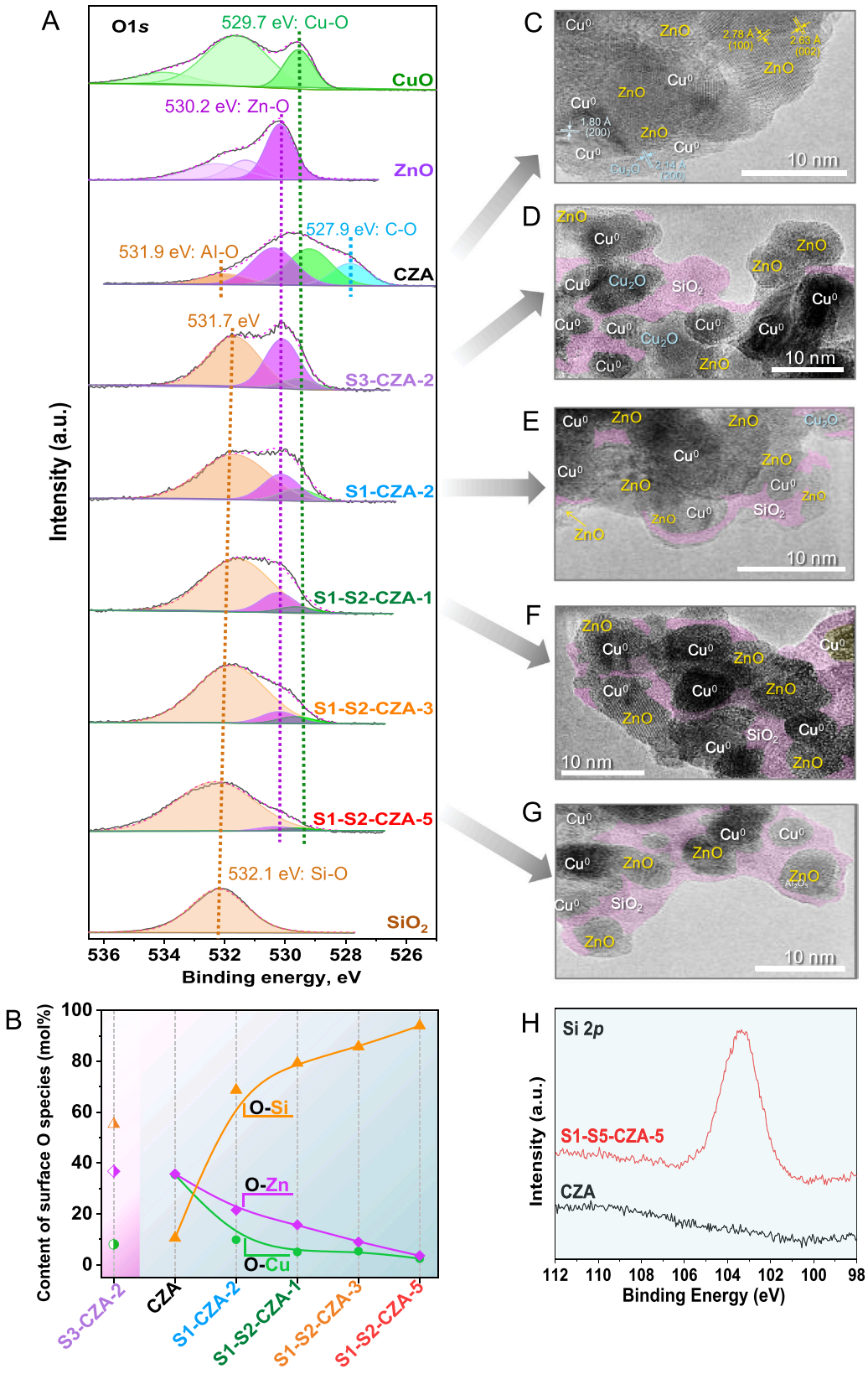

Fig. 4. Location of SiO_2 species on the catalyst surface. (A) O 1 *s* XPS spectra of calcined catalysts and (B) the corresponding fitted results; HREM images of used catalyst: (C) CZA, (D) S3-CZA-*2*, (E) S1-CZA-*2*, (F) S1-S2-CZA-*1*, (G) S1-S2-CZA-*5* (the amorphous SiO_2 in the images was colored with pink), (H) Si 2*p* XPS spectra of used catalyst.

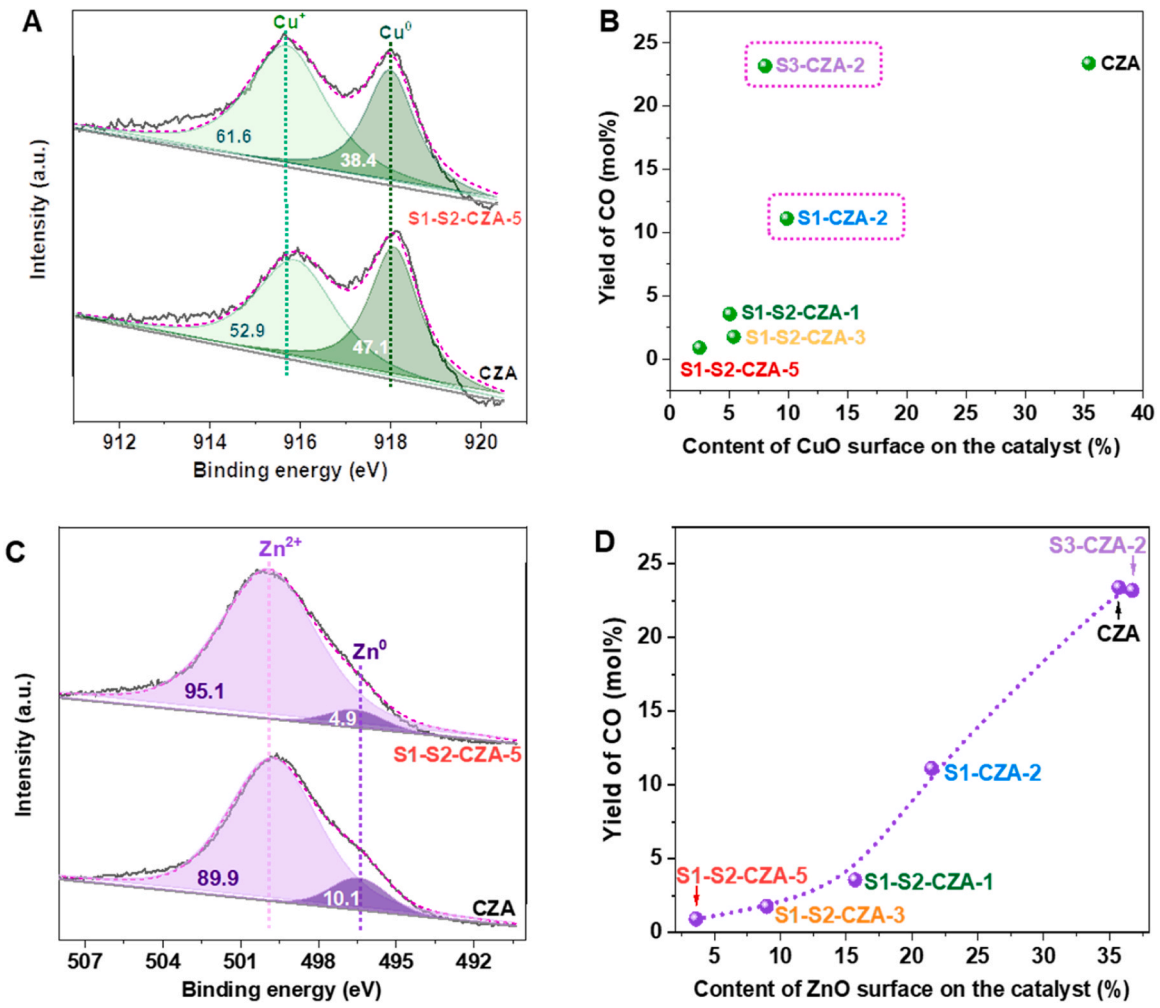

Fig. 5. Effect of Si species on the catalyst reduction and Correlation of catalyst surface with CO yield: (A) in situ Cu LMM XAES and (C) in situ Zn LMM XAES spectra of reduced catalyst. Correlations of (B) CuO surface content and (D) ZnO surface content with CO yield, respectively (Contents of CuO surfaces were detected by O 1 *s* XPS, as shown in Fig. 4B).

higher temperatures on the silylated catalysts (Fig. S12A in ESI). The presence of surface SiO_2 species delayed the reduction of CuO to Cu^0. Noticeably, the maximal reduction temperature for all of the silylated catalysts were less or close to 250 °C, except for S1-S2-CZA-*5*. As the catalysts in this work was reduced in H_2/Ar at 250 °C for a long duration of 10 h, it is reasonable to deduce that this reduction condition enabled the reduction of CuO in the catalysts to Cu^0 and the reduction degree of the silylated catalysts (except S1-S2-CZA-*5*) were comparable to that of CZA.

For S1-S2-CZA-*5*, its maximal temperature for reducing CuO to Cu^0 reached 262.7 °C, as displayed by H_2-TPR. To explore the reduction degree of Cu on it, in situ XPS analysis was performed (Fig. 5A, Fig. S13 in ESI). The Cu LMM XAES results indicated that the surface Cu^0 (centered at 918.0 eV [42]) on the reduced S1-S2-CZA-*5* reached 38.4%, which maintained at a similar level to that of CZA (47.1%). This result indicated the majority of CuO can reduced to Cu^0 even covered by SiO_2 species. As displayed in HRTEM, the SiO_2 species were mesoporous, which enabled the transfer of H_2 through the SiO_2 layers and thus the reduction of CuO.

It is demonstrated that the Cu-SiO_2 interface with the Cu-O-Si interface had a catalytic role in hydrogenation reactions [43,44]. In this work, the SiO_2 species was grafted on the CuO NPs via interacting with the surface hydroxyls (Cu-OHs) during the silyation. The Cu-SiO_2 interface was inevitably formed with the Cu-O-Si structure. This is confirmed by the Cu 2*p* XPS analysis, as the formation of Cu-O-Si led to the shift of Cu 2*p* peak to high binding energy direction (Fig. S14 in ESI). The contribution of Cu-SiO_2 interface to the CO formation was not obvious. As indicated by the O 1 *s* XPS result, the coverage of SiO_2 species on the CuO surface was close on both S1-CZA-*2* and S3-CZA-*2* catalysts, indicating the comparable Cu-SiO_2 interface on the two catalysts. However, their CO yield largely varied (Fig. 5B).

Noticeably, the CO yield was positively related to the content of ZnO surface for all of the catalysts. As the ZnO surface was gradually covered by the SiO_2 species, the CO yield on the catalysts decreased accordingly (Fig. 5D). This positive correlation implies that the SiO_2 species located on the ZnO surface suppressed the CO formation. Hydrogen (H) spillover from Cu^0 sites to the supports has been long reported for the CO_2-to-methanol Cu-based catalysts [45–48], and the hydroxyls are known as the transporter for H spillover [33,45,49–52]. We therefore hypothesized that for CZA catalyst, the active H species can transfer from Cu^0 to ZnO via the OHs on the ZnO surface (designated as Zn-OHs), accelerating RWGS reaction to produce CO. For the silylated catalysts, the SiO_2 species was grafted on the ZnO surface via the surface Zn-OHs. In such case, the consumption of Zn-OHs by silylation will disfavor H spillover and RWGS reaction.

The H spillover from Cu^0 onto ZnO was observed by in situ Zn LMM and H_2-TPR analysis. The H_2-TPR result showed that ZnO in CZA was reduced to Zn^0 (metallic Zn) with a high peak temperature of 593.3 °C (Fig. S12B in ESI), in good agreement with the literature [25]. Considering the low temperature for catalyst reduction in this work (250 °C for

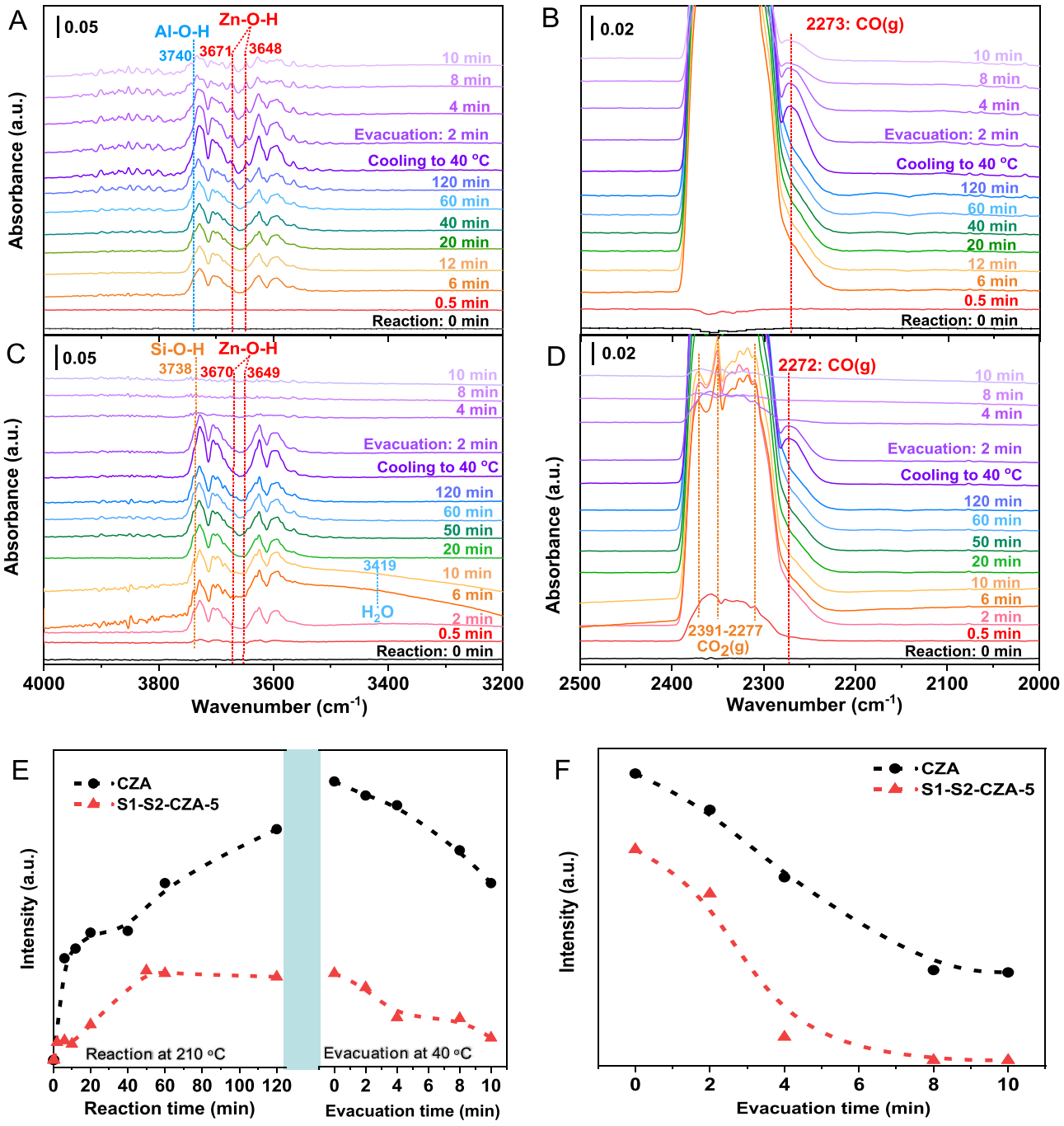

Fig. 6. *In situ* DRIFT spectra of the regions of OH groups and CO over: (A-B) CZA, (C-D) S1-S2-CZA-*5*. (From bottom to top: reaction at 210 °C from 0 to 120 min, followed by cooling down to 40 °C and evacuation at 40 °C from 0 to 10 min); (E) Variation of Zn-OH peak intensity (at ca. 3670 cm^{-1}) over CZA and S1-S2-CZA-*5* (From left to right: reaction at 210 °C from 0 to 120 min, followed by cooling down to 40 °C and evacuation at 40 °C from 0 to 10 min); (F) Variation of CO peak intensity (at ca. 2272 cm^{-1}) over CZA and S1-S2-CZA-*5* after cooling to 40 °C and evacuation at 40 °C from 0 to 10 min).

10 h in H_2/Ar), it is difficult for ZnO itself in CZA to reduce to Zn^0. However, in situ Zn LMM analysis showed that 10.1% of ZnO in CZA was reduced to Zn^0, with the peak centered at 496.4 eV [53] (Fig. 5C). This acceleration in the reduction of ZnO is indicative of H overflow from Cu^0 onto ZnO. The active H species that generated from Cu^0 sites can diffuse onto ZnO, accelerating the reduction of ZnO. Compared with CZA, the amount of Zn^0 was largely reduced to 4.9% over S1-S2-CZA-*5*. 91.0% of the ZnO surface on S1-S2-CZA-*5* was covered by the SiO_2 species (as indicated by the O 1 *s* XPS analysis in Fig. 4A-4B), troubling H transfer from Cu^0 onto ZnO. The suppression of H spillover was also observed on the other silylated catalysts, except for S3-CZA-*2*. As shown in Fig. S12B in ESI, the reduction of ZnO to Zn^0 completed at higher temperatures for the silyated catalysts than CZA. Whereas for S3-CZA-*2*, its ZnO surface was not covered by the SiO_2 species, leaving the Zn-OHs for the transfer of active H species. Hence, the reduction of ZnO on S3-CZA-*2* was comparable to that on CZA.

The H spillover on the catalyst was also evidenced by H_2-TPR on the silylated catalysts with introduced Fe_2O_3 species (Fig. S15 in ESI). It has been reported that for the Pt-Fe/Al_2O_3 supported catalyst, overflowing of the H species generated on platinum NPs onto Al_2O_3 could promote the reduction of Fe_2O_3 NPs [54]. In such case, the Fe_2O_3 NPs can act as an indicator for H spillover. In this work, the Fe_2O_3 species was

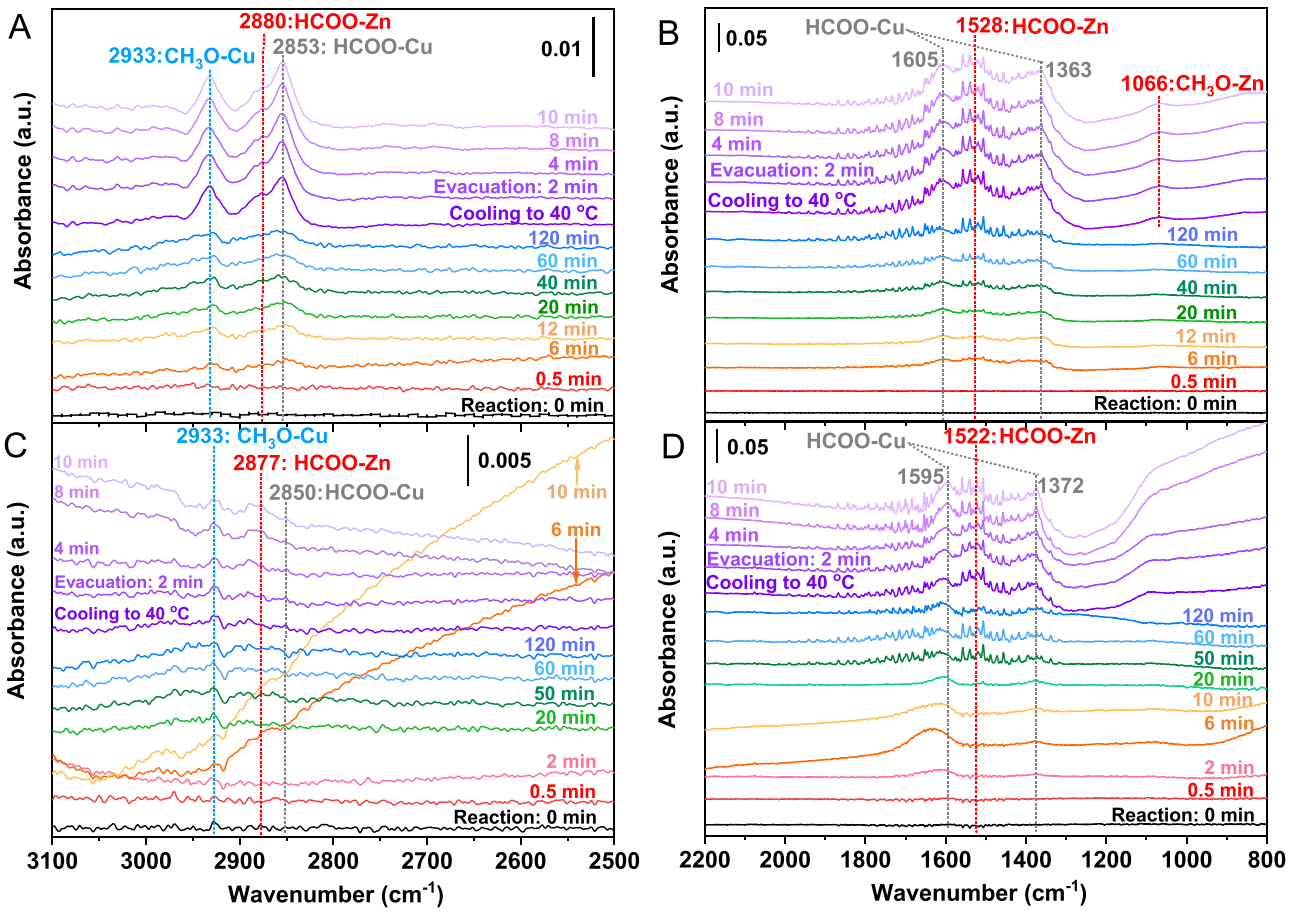

Fig. 7. *In situ* DRIFT spectra of the regions of HCOO and CH_3O species over: (A-B) CZA, (C-D) S1-S2-CZA-*5*. (From bottom to top: reaction at 210 °C from 0 to 120 min, followed by cooling down to 40 °C and evacuation at 40 °C from 0 to 10 min).

introduced into the pristine and silylated CZA catalysts via the impregnation method (detailed in ESI). In the case that H spillover on the silylated catalyst surface is suppressed, the reduction of Fe_2O_3 will become difficult. Indeed, the reduction peak of Fe_2O_3 to Fe_3O_4 appeared at ca. 364.0 °C on CZA, which gradually moved to 462.5 °C on the silylated catalysts (Fig. S15B in ESI).

In situ DRIFT spectroscopy was performed to gain more mechanical insight into the Zn-OH promoted RWGS reaction over CZA and S1-S2-CZA-*5* (Fig. 6). As the overflow of H from Cu^0 to ZnO will produce new surface Zn-OH groups, the OH region at 3500–3800 cm^{-1} on the two catalysts was monitored during the reaction (Fig. 6A, C). Two OH peaks at ca. 3670 and 3649 cm^{-1} appeared on CZA and S1-S2-CZA-*5* after reaction for 120 min, in accordance with the OH species on ZnO [55]. To accurately assign the two peaks, the OH region on Cu/ZnO and Cu/SiO_2 model catalysts were also detected after the reaction. The two OH peaks are present on Cu/ZnO but absent on Cu/SiO_2, proofing their assignation to the Zn-OH species (Fig. S16 in ESI). Besides, their intensities substantially declined when evacuating at 210 °C, further supporting their attribution to the Zn-OH species (Fig. S17 in ESI). Noticeably, the intensity of Zn-OH peaks on CZA appeared and linearly increased with the reaction time, implying the H spillover from Cu^0 to ZnO promoted the formation of new Zn-OH groups; whereas it grew slowly till reacting for 50 min and maintained at a low value thereafter on S1-S2-CZA-*5*, clearly demonstrating the suppression effect of surface silylation on the H overflow from Cu^0 to ZnO (Fig. 6A, C, E).

The CO peak was absent on CZA and S1-S2-CZA-*5* during reaction at 210 °C, probably due to that the weak adsorption of CO on the Cu-based catalyst facilitates the fast diffusion of CO from the reaction system [33, 42] (Fig. 6B, 6D). To slow down the diffusion of CO, the reaction system was cooled down to 40 °C, on which the characteristic peak of gaseous CO (g) species appeared at ca. 2276 cm^{-1} [33,56,57]. Noticeably, the intensity of CO (g) peak gradually reduced after evacuation at 40 °C for 10 min, accompanied by the decrease in the Zn-OHs on the both catalysts (Fig. 6F). The positive correlation of CO formation with the Zn-OHs is in good agreement with the XPS result, both demonstrating the Zn-OH promoted RWGS reaction mechanism.

Moreover, the key reaction intermediates over CZA and S1-S2-CZA-*5* were monitored by in situ DRIFT spectroscopy. The typical DRIFT assignments of surface species on the CO_2-to-methanol catalysts in literature are listed in Table S6 in ESI for reference. As displayed in Fig. 7, the bands at ca. 2853, 1605, and 1363 cm^{-1}, and the bands at about 2880 and 1528 cm^{-1}, characteristic of the copper formate (*HCOO-Cu) and zinc formate (*HCOO-Zn) [42,58], respectively, appeared and gradually intensified with the reaction time. Meanwhile, the peaks attributed to the copper methoxide (*CH_3O-Cu) and the zinc methoxide (*CH_3O-Zn) were found at ca. 2933 and 1066 cm^{-1}, respectively [42,58]. These results indicate the methanol formation via the formate pathway.

To describe the H spillover from Cu^0 onto ZnO via the Zn-OHs and further understand its catalytic role in CO_2 hydrogenation, DFT calculation was performed on ZnO/Cu (111) model to represent the ZnO-Cu interface without Zn-OHs and Zn-OH/Cu (111) to model the surface with a Zn-OH (Fig. S18 in ESI). Based on the in situ XPS/DRIFT results and the findings in literature [1,59], the formate route was preferentially considered for CO_2 hydrogenation to methanol via *HCOO, *HCOOH, *H_2COOH, and *H_3CO intermediate, while the reaction pathway for RWGS reaction was proceeded via a *HOCO intermediate to produce CO (Fig. 6, Fig. S19-S20 in ESI).

As indicated by DFT calculations, the rate-limiting step for CO

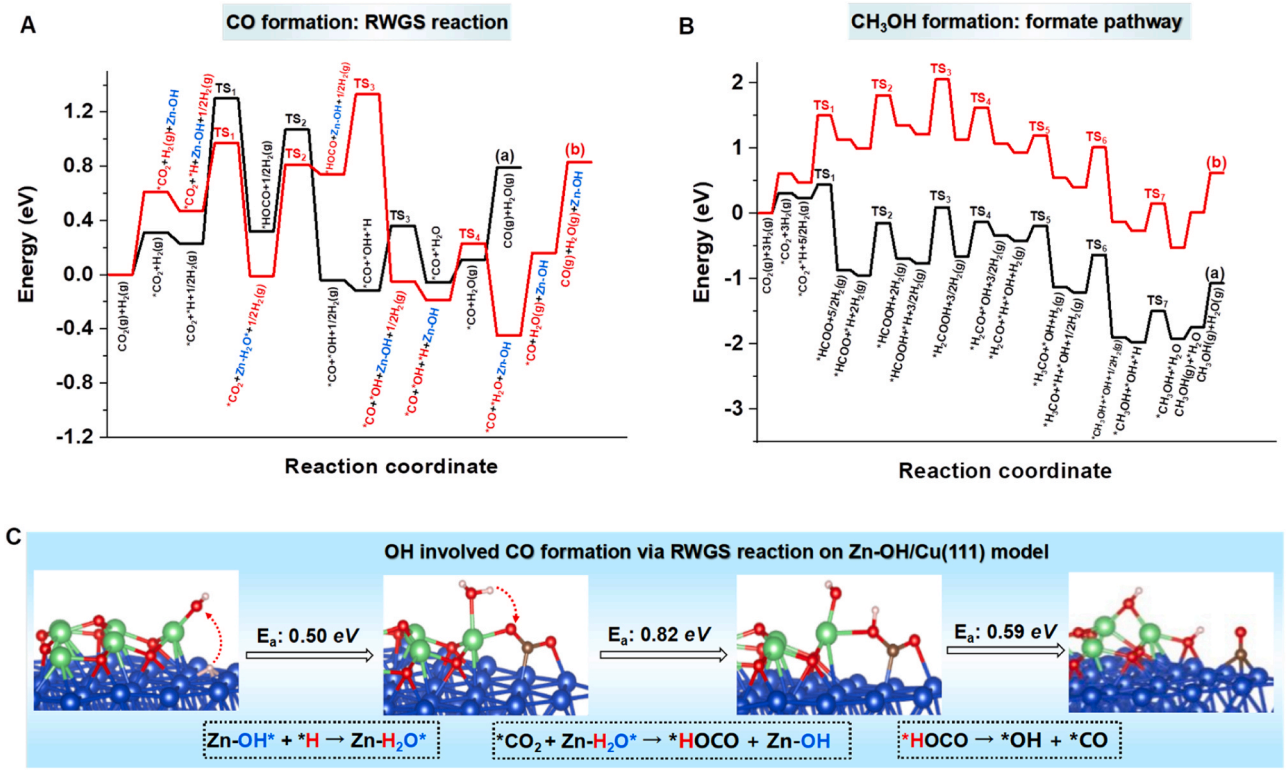

Fig. 8. Potential energy diagrams: (A) Hydrogenation of CO_2(g) to CO(g) (a: on ZnO/Cu(111), b: on Zn-OH/Cu(111)). (B) CO_2(g) hydrogenation to CH_3OH(g) (a: on ZnO/Cu(111), b: on Zn-OH/Cu(111)). TS, transition state. (**C**) The Zn-OH involved CO formation via RWGS reaction on Zn-OH/Cu (111) model. Cu, blue; Zn, green; O, red; H, white; C, gray.

formation was hydrogenation of CO_2 to *HOCO ($*CO_2 + *H \rightarrow *HOCO$) on both models, while that for methanol formation was shifted from the step of $*HCOOH \rightarrow *H_2COOH$ on ZnO/Cu (111) model to the step of $*CO_2 + *H \rightarrow *HCOO$ on Zn-OH/Cu (111) model (Fig. 8, Tables S7 and S8 in ESI). On ZnO/Cu (111) model, the activation energy (E_a) for methanol formation is 0.86 eV; CO formation is unfavorable compared with methanol formation, due to the higher E_a (1.07 eV) of the rate-limiting step (Fig. 8A-8B, Tables S3 in ESI). On Zn-OH/Cu (111) model, a *H species generated on Cu sites can readily diffuse onto a Zn-OH group with low E_a of 0.50 eV, forming a Zn-H_2O* coordination species. The Zn-H_2O* species delivers this *H species to interact with CO_2, not only making the formation of *HOCO kinetically favorable (E_a = 0.82 eV), but also recovering itself as a Zn-OH group for the catalytic cycle (Fig. 8, Table S8 in ESI). Compared with that for CO formation, the rate-limiting step for methanol formation on Zn-OH/Cu (111) has higher E_a (1.03 eV) (Fig. 8, Table S8 in ESI), indicating that CO formation is a more preferred pathway. Thus, the DFT results confirmed the presence of H spillover from Cu to ZnO via the Zn-OHs, which agrees well with the above experimental observations. Moreover, the spilled H species participated in RWGS reaction and promoted the CO formation.

4. Conclusion

We have presented a simply surface silylation way to efficiently suppress CO formation on a commercial $Cu/ZnO/Al_2O_3$ catalyst in CO_2 hydrogenation to methanol. In this method, the joint silyation with hexamethyl disiloxane and tetraethyl orthosilicate enabled almost the complete coverage of the hydroxyls on the ZnO component (Zn-OHs), minimizing RWGS activity and thus optimizing methanol selectivity. The characterization methods and DFT calculations support a RWGS cycle that involves the delivery of active hydrogen atoms from Cu to the reactants via the Zn-OHs, and further a RWGS suppression mechanism by coverage of the Zn-OHs via surface silylation. More generally, the ability of surface silylation demonstrated here to regulate RWGS reaction is also expected in WGS reaction that is a reverse reaction of RWGS. We envision that the surface silylation method will benefit the development and optimization of catalysts with surface hydroxyls for the processes involving RWGS or WGS reaction.

CRediT authorship contribution statement

Xiaojing Cui: Writing and editing of the original and revised manuscript, data curation and investigation. Yequn Lin: HRTEM analysis of catalysts. Wenjun Yan: XPS analysis of catalysts. Yanfeng Xue: visualization. Yangang Mei: data calculation and TG analysis. Jiamei Li: validation. Xiaoqing Gao: validation. He Zhang: writing (review and editing). Shanhui Zhu: DFT calculation, review and editing. Yulan Niu: supervision, resources and investigation. Tiansheng Deng: methodology, conceptualization, project administration, writing (review and editing).

Declaration of Competing Interest

The authors declare that they have no known competing financial interests or personal relationships that could have appeared to influence the work reported in this paper.

Data Availability

Data will be made available on request.

Acknowledgements

This work was supported by the National Natural Science Foundation of China (grant numbers: 21972159, 21303240), the Fund for Shanxi "1331 project", the Fund for Scientific and Technological Innovation Programs of Higher Education Institutions in Shanxi (grant number:

2021L536), Program for the Discipline Leaders of Taiyuan Institute of Technology and the Fund for Innovation and Entrepreneurship Project for College Students (grant number: 20221194).

Appendix A. Supporting information

Supplementary data associated with this article can be found in the online version at doi:10.1016/j.apcatb.2023.123099.

References

[1] S. Kattel, J.G. Chen, J.A. Rodriguez, P. Liu, Active sites for CO_2 hydrogenation to methanol on Cu/ZnO catalysts, Science 355 (2017) 1296–1299, https://doi.org/10.1126/science.aal3573.

[2] J. Niu, H. Liu, Y. Jin, B. Fan, W. Qi, J. Ran, Comprehensive review of Cu-based CO_2 hydrogenation to CH_3OH: insights from experimental work and theoretical analysis, Int. J. Hydrog. Energ. 47 (2022) 9183–9200, https://doi.org/10.1126/science.aal3573.

[3] K. Wang, Y. Du, Y. Li, X. Wu, H. Hu, G. Wang, Y. Xiao, S. Chou, G. Zhang, Atomic-level insight of sulfidation-engineered Aurivillius-related $Bi_2O_2SiO_3$ nanosheets enabling visible light low-concentration CO_2 conversion, Carbon Energy 5 (2023), e264, https://doi.org/10.1002/cey2.264.

[4] K. Wang, H. Qin, J. Li, Q. Cheng, Y. Zhu, H. Hu, J. Peng, S. Chen, G. Wang, S. Chou, S. Dou, Y. Xiao, Metallic $AgInS_2$ nanocrystals with sulfur vacancies boost atmospheric CO_2 photoreduction under near-infrared light illumination, Appl. Catal. B: Environ. 332 (2023), 122763, https://doi.org/10.1016/j.apcatb.2023.122763.

[5] K. Wang, Q. Wang, K. Zhang, G. Wang, H. Wang, Selective solar-driven CO_2 reduction mediated by 2D/2D $Bi_2O_2SiO_3$/MXene nanosheets heterojunction, J. Mater. Sci. Technol. 124 (2022) 202–208, https://doi.org/10.1016/j.jmst.2021.10.059.

[6] K. Wang, H. Qin, X. Shao, L. Jiang, K. Li, J. Wang, L. Zhou, Q. Cheng, G. Wang, H. Wang, Unveiling S-scheme charge transfer pathways in In_2S_3/Nb_2O_5 hybrid nanofiber photocatalysts for low-concentration CO_2 hydrogenation, Sol. Rrl. 7 (2023), 2200963, https://doi.org/10.1002/solr.202200963.

[7] Y. Shi, Y. Zhou, Y. Lou, Z. Chen, H. Xiong, Y. Zhu, Homogeneity of supported single-atom active sites boosting the selective catalytic transformations, Adv. Sci. 9 (2022), 2201520, https://doi.org/10.1002/advs.202201520.

[8] C. Yao, H. Fan, A. Adogwa, H. Xiong, M. Yang, F. Liu, Z. Chen, Y. Lou, Recent advances in carbon dioxide selective hydrogenation and biomass valorization via single-atom catalysts, Resour. Chem. Mater. 2 (2023) 189–207, https://doi.org/10.1016/j.recm.2023.05.003.

[9] Y. Ni, Z. Chen, Y. Fu, Y. Liu, W. Zhu, Z. Liu, Selective conversion of CO_2 and H_2 into aromatics. Nat. Commun. 9 (2018) 3457, https://doi.org/10.1038/s41467-018-05880-4.

[10] P. Gao, X. Bu, S. Dang, Z. Liu, H. Wang, L. Zhong, M. Qiu, C. Yang, J. Cai, W. Wei, Y. Sun, Direct conversion of CO_2 into liquid fuels with high selectivity over a bifunctional catalyst, Nat. Chem. 9 (2017) 1019–1024, https://doi.org/10.1038/nchem.2794.

[11] Y. Lou, F. Jiang, W. Zhu, L. Wang, T. Yao, S. Wang, B. Yang, B. Yang, Y. Zhu, X. Liu, CeO_2 supported Pd dimers boosting CO_2 hydrogenation to ethanol, Appl. Catal. B: Environ. 291 (2021), 120122, https://doi.org/10.1016/j.apcatb.2021.120122.

[12] G. Bonura, M. Cordaro, C. Cannilla, F. Arena, F. Frusteri, The changing nature of the active site of Cu-Zn-Zr catalysts for the CO_2 hydrogenation reaction to methanol, Appl. Catal. B: Environ. 152–153 (2014) 152–161, https://doi.org/10.1016/j.apcatb.2014.01.035.

[13] X. Dong, N. Zhao, F. Xiao, J. Wang, Y. Tan, CO_2 hydrogenation to methanol over Cu/ZnO/ZrO_2 catalysts prepared by precipitation-reduction method, Appl. Catal. B Environ. 191 (2016) 8–17, https://doi.org/10.1016/j.apcatb.2016.03.014.

[14] K. Chen, S. Wu, X. Liu, J. Zheng, S. Zhou, X. Duan, Y. Zhuang, S.C.E. Tsang, Y. Yuan, CO_2 hydrogenation to methanol over Cu catalysts supported on La-modified SBA-15: the crucial role of Cu-LaOx interfaces, Appl. Catal. B Environ. 251 (2019) 119–129, https://doi.org/10.1016/j.apcatb.2019.03.059.

[15] S. Chen, J. Zhang, F. Song, Q. Zhang, G. Yang, M. Zhang, X. Wang, H. Xie, Y. Tan, Induced high selectivity methanol formation during CO_2 hydrogenation over a $CuBr_2$-modified CuZnZr catalyst, J. Catal. 389 (2020) 47–59, https://doi.org/10.1016/j.jcat.2020.05.023.

[16] N. Rui, Z. Wang, K. Sun, J. Ye, Q. Ge, C. Liu, CO_2 hydrogenation to methanol over Pd/In_2O_3: effects of Pd and oxygen vacancy, Appl. Catal. B: Environ. 218 (2017) 488–497, https://doi.org/10.1016/j.apcatb.2017.06.069.

[17] J. Song, S. Liu, C. Yang, G. Wang, H. Tian, Z. Zhao, R. Mu, J. Gong, The role of Al doping in Pd/ZnO catalyst for CO_2 hydrogenation to methanol, Appl. Catal. B: Environ. 263 (2020), 118367, https://doi.org/10.1016/j.apcatb.2019.118367.

[18] J. Wang, G. Li, Z. Li, C. Tang, Z. Feng, H. An, H. Liu, T. Liu, C. Li, A highly selective and stable ZnO-ZrO_2 solid solution catalyst for CO_2 hydrogenation to methanol, Sci. Adv. 3 (2017), e1701290, https://doi.org/10.1126/sciadv.1701290.

[19] M. Behrens, I. Kasatkin, S. Kühl, M. Hävecker, F. Abild-Pedersen, S. Zander, F. Girgsdies, P. Kurr, B.-L. Kniep, M. Tovar, R.W. Fischer, J.K. Nørskov, R. Schlögl, The active site of methanol synthesis over Cu/ZnO/Al_2O_3 industrial catalysts, Science 336 (2012) 893–897, https://doi.org/10.1126/science.1219831.

[20] J.S. Lee, K.H. Lee, S.Y. Lee, Y.G. Lee, A comprehensive study of methanol synthesis from CO_2/H_2 and CO/H_2 over a Cu/ZnO/Al_2O_3 catalyst, J. Catal. 144 (1993) 414–424, https://doi.org/10.1006/jcat.1993.1342.

[21] K.-W. Jun, W.-J. Shen, K.S. Rama Rao, K.-W. Lee, Residual sodium effect on the catalytic activity of Cu/ZnO/Al_2O_3 in methanol synthesis from CO_2 hydrogenation, Appl. Catal. A: Gen. 174 (1998) 231–238, https://doi.org/10.1016/S0926-860X(98)00195-1.

[22] J. Deng, Q. Sun, Y. Zhang, S. Chen, D. Wu, A novel process for preparation of a Cu/ZnO/Al_2O_3 ultrafine catalyst for methanol synthesis from $CO_2 + H_2$: comparison of various preparation methods, Appl. Catal. A: Gen. 139 (1996) 75–85, https://doi.org/10.1016/0926-860X(95)00324-X.

[23] Q. Sun, Y.-L. Zhang, H.-Y. Chen, J.-F. Deng, D. Wu, S.-Y. Chen, A novel process for the preparation of Cu/ZnO and Cu/ZnO/Al_2O_3 ultrafine catalyst: structure, surface properties, and activity for methanol synthesis from $CO_2 + H_2$, J. Catal. 167 (1997) 92–105, https://doi.org/10.1006/jcat.1997.1554.

[24] Z. Hong, Y. Gao, J. Deng, K. Fan, CO_2 hydrogenation to methanol over Cu/ZnO/Al_2O_3 catalyts prepared by a novel gel-network-coprecipitation method, Catal. Lett. 82 (2002) 37–44, https://doi.org/10.1023/A:1020531822590.

[25] F. Liao, Y. Huang, J. Ge, W. Zheng, K. Tedsree, P. Collier, X. Hong, S.C. Tsang, Morphology-dependent interactions of ZnO with Cu nanoparticles at the materials: interface in selective hydrogenation of CO_2 to CH_3OH, Angew. Chem. 123 (2011) 2210–2213, https://doi.org/10.1002/anie.201007108.

[26] V.D.B.C. Dasireddy, B. Likozar, The role of copper oxidation state in Cu/ZnO/Al_2O_3 catalysts in CO_2 hydrogenation and methanol productivity, Renew. Energ. 140 (2019) 452–460, https://doi.org/10.1016/j.renene.2019.03.073.

[27] H. Li, L. Wang, X. Gao, F. Xiao, Cu/ZnO/Al_2O_3 catalyst modulated by zirconia with enhanced performance in CO_2 hydrogenation to methanol, Ind. Eng. Chem. Res. 61 (2022) 10446–10454, https://doi.org/10.1021/acs.iecr.2c00172.

[28] Q. Guo, S. Li, J. Li, Y. Hu, C. Duanmu, Enhanced CO_2 hydrogenation to methanol on the mesostructured Cu-ZnO/Al_2O_3-ZrO_2 catalyst, ACS Appl. Energy Mater. 4 (2021) 8311–8321, https://doi.org/10.1021/acsaem.1c01542.

[29] P. Gao, L. Zhong, L. Zhang, H. Wang, N. Zhao, W. Wei, Y. Sun, Yttrium oxide modified Cu/ZnO/Al_2O_3 catalysts via hydrotalcite-like precursors for CO_2 hydrogenation to methanol, Catal. Sci. Technol. 5 (2015) 4365–4377, https://doi.org/10.1039/c5cy00372e.

[30] Q. Ma, M. Geng, J. Zhang, X. Zhang, T.-S. Zhao, Enhanced catalytic performance for CO_2 hydrogenation to methanol over N-doped graphene incorporated Cu-ZnO-Al_2O_3 catalysts, ChemistrySelect 4 (2019) 78–83, https://doi.org/10.1002/slct.201803186.

[31] T. Qi, Y. Zhao, S. Chen, W. Li, X. Guo, Y. Zhang, C. Song, Bimetallic metal organic framework-templated synthesis of a Cu-ZnO/Al_2O_3 catalyst with superior methanol selectivity for CO_2 hydrogenation, Mol. Catal. 514 (2021), 111870, https://doi.org/10.1016/j.mcat.2021.111870.

[32] W. Yue, Y. Li, W. Wei, J. Jiang, J. Caro, A. Huang, Highly selective CO_2 conversion to methanol in a bifunctional zeolite catalytic membrane reactor, Angew. Chem. Int. Ed. 60 (2021) 18289–18294, https://doi.org/10.1002/anie.202106277.

[33] X. Cui, S. Chen, H. Yang, Y. Liu, H. Wang, H. Zhang, Y. Xue, G. Wang, Y. Niu, T. Deng, W. Fan, Improving methanol selectivity in CO_2 hydrogenation by tuning the distance of Cu on catalyst, Appl. Catal. B: Environ. 298 (2021), 120590, https://doi.org/10.1016/j.apcatb.2021.120590.

[34] X. Cui, W. Yan, H. Yang, Y. Shi, Y. Xue, H. Zhang, Y. Niu, W. Fan, T. Deng, Preserving the active Cu–ZnO interface for selective hydrogenation of CO_2 to dimethyl ether and methanol, ACS Sustain. Chem. Eng. 9 (2021) 2661–2672, https://doi.org/10.1021/acssuschemeng.0c07258.

[35] H. Ruland, H. Song, D. Laudenschleger, S. Stürmer, S. Schmidt, J. He, K. Kähler, M. Muhler, R. Schlögl, CO_2 hydrogenation with Cu/ZnO/Al_2O_3: a benchmark study, ChemCatChem 12 (2020) 3216–3222, https://doi.org/10.1002/cctc.202000195.

[36] A. Prašnikar, D.L. Jurković, B. Likozar, Reaction path analysis of CO_2 reduction to methanol through multisite microkinetic modelling over Cu/ZnO/Al_2O_3 catalysts, Appl. Catal. B: Environ. 292 (2021), 120190, https://doi.org/10.1016/j.apcatb.2021.120190.

[37] G. Kresse, J. Hafner, Ab initiomolecular dynamics for liquid metals, Phys. Rev. B 47 (1993) 558–561, https://doi.org/10.1103/PhysRevB.47.558.

[38] J.P. Perdew, Y. Wang, Accurate and simple analytic representation of the electron-gas correlation energy, Phys. Rev. B 45 (1992) 13244–13249, https://doi.org/10.1103/PhysRevB.45.13244.

[39] G. Kresse, D. Joubert, From ultrasoft pseudopotentials to the projector augmented-wave method, Phys. Rev. B 59 (1999) 1758–1775, https://doi.org/10.1103/PhysRevB.59.1758.

[40] G. Henkelman, B.P. Uberuaga, H. Jónsson, A climbing image nudged elastic band method for finding saddle points and minimum energy paths, J. Chem. Phys. 113 (2000) 9901–9904, https://doi.org/10.1063/1.1329672.

[41] R. Rajendran, L.K. Shrestha, K. Minami, M. Subramanian, R. Jayavel, K. Ariga, Dimensionally integrated nanoarchitectonics for a novel composite from 0D, 1D, and 2D nanomaterials: RGO/CNT/CeO_2 ternary nanocomposites with electrochemical performance, J. Mater. Chem. A 2 (2014) 18480–18487, https://doi.org/10.1039/c4ta03996c.

[42] H. Yang, Y. Chen, X. Cui, G. Wang, Y. Cen, T. Deng, W. Yan, J. Gao, S. Zhu, U. Olsbye, J. Wang, W. Fan, A highly stable copper-based catalyst for clarifying the catalytic roles of Cu^0 and Cu^+ species in methanol dehydrogenation, Angew. Chem. 130 (2018) 1854–1858, https://doi.org/10.1002/ange.201710605.

[43] X. Gong, M. Wang, H. Fang, X. Qian, L. Ye, X. Duan, Y. Yuan, Copper nanoparticles socketed in situ into copper phyllosilicate nanotubes with enhanced performance for chemoselective hydrogenation of esters, Chem. Commun. 53 (2017) 6933–6936, https://doi.org/10.1039/C7CC02093G.

[44] W. Di, J. Cheng, S. Tian, J. Li, J. Chen, Q. Sun, Synthesis and characterization of supported copper phyllosilicate catalysts for Acetic Ester Hydrogenation to

Ethanol, Appl. Catal. A Gen. 510 (2016) 244–259, https://doi.org/10.1016/j.apcata.2015.10.026.
[45] R. Burch, S.E. Golunski, M.S. Spencer, The role of copper and zinc oxide in methanol synthesis catalysts, J. Chem. Soc., Faraday Trans. 86 (1990) 2683–2691, https://doi.org/10.1039/ft9908602683.
[46] K. Fujimoto, Y. Yu, Spillover effect on the stabilization of Cu-Zn catalyst for CO_2 hydrogenation to methanol, Stud. Surf. Sci. Catal. 77 (1993) 393–396, https://doi.org/10.1016/S0167-2991(08)63219-X.
[47] K.-D. Jung, A.T. Bell, Role of hydrogen spillover in methanol synthesis over Cu/ZrO_2, J. Catal. 193 (2000) 207–223, https://doi.org/10.1006/jcat.2000.2881.
[48] B. Hu, Y. Yin, G. Liu, S. Chen, X. Hong, S.C.E. Tsang, Hydrogen spillover enabled active Cu sites for methanol synthesis from CO_2 hydrogenation over Pd doped CuZn catalysts, J. Catal. 359 (2018) 17–26, https://doi.org/10.1016/j.jcat.2017.12.029.
[49] D.H. Lenz, W.C. Conner, Hydrogen spillover on silica: ethylene hydrogenation and H_2-D_2 exchange, J. Catal. 104 (1987) 288–298, https://doi.org/10.1016/0021-9517(87)90360-5.
[50] D.H. Lenz, W.C. Conner, Hydrogen spillover on silica: II. Kinetics and mechanism of the induction of catalytic activity, J. Catal. 112 (1988) 116–125, https://doi.org/10.1016/0021-9517(88)90125-x.
[51] R. Burch, R.J. Chappellt, S.E. Golunski, Synergy between copper and zinc oxide during methanol synthesis. Transfer of activating species, J. Chem. Soc. Faraday Trans. 1 (85) (1989) 3569–3578, https://doi.org/10.1039/f19898503569.
[52] F. Sha, S. Tang, C. Tang, Z. Feng, J. Wang, C. Li, The role of surface hydroxyls on ZnZrOx solid solution catalyst in CO_2 hydrogenation to methanol, Chinese, J. Catal. 45 (2023) 162–173, https://doi.org/10.1016/S1872-2067(22)64176-7.
[53] S. Kuld, C. Conradsen, Poul Georg Moses, Ib Chorkendorff, Jens Sehested, Quantification of zinc atoms in a surface alloy on copper in an industrial-type methanol synthesis catalyst, Angew. Chem. 53 (2014) 5941–5945, https://doi.org/10.1002/anie.201311073.
[54] W. Karim, C. Spreafico, A. Kleibert, J. Gobrecht, J.V. Vondele, Y. Ekinci, J.A. van Bokhoven, Catalyst support effects on hydrogen spillover, Nature 541 (2017) 68–71, https://doi.org/10.1038/nature20782.
[55] L. Zhang, X. Zhang, K. Qian, Z. Li, Y. Cheng, L.L. Daemen, Z. Wu, W. Huang, Activation and surface reactions of CO and H_2 on ZnO powders and nanoplates under CO hydrogenation reaction conditions, J. Energ. Chem. 50 (2020) 351–357, https://doi.org/10.1016/j.jechem.2020.03.038.
[56] R. Burch, S. Chalker, J. Pritchard, In situ fourier-transform infrared investigation of the interaction of CO-CO_2-H_2 with Cu catalysts at low temperatures and high pressures, J. Chem. Soc. Faraday Trans. 87 (1991) 1791–1794, https://doi.org/10.1039/FT9918701791.
[57] I.A. Fisher, A.T. Bell, In situ infrared study of methanol synthesis from H_2/CO over Cu/SiO_2 and Cu/ZrO_2/SiO_2, J. Catal. 178 (1998) 153–173, https://doi.org/10.1016/jcat.1998.2134.
[58] S. Fujita, M. Usui, H. Ito, N. Takezawa, Mechanisms of methanol synthesis from carbon dioxide and from carbon monoxide at atmosphere pressure over Cu/ZnO, J. Catal. 157 (1995) 403–413, https://doi.org/10.1006/jcat.1995.1306.
[59] Y. Yang, J. Evans, J.A. Rodriguez, M.G. White, P. Liu, Fundamental studies of methanol synthesis from CO_2 hydrogenation on Cu(111), Cu clusters, and Cu/ZnO (0001), Phys. Chem. Chem. Phys. 12 (2010) 9909–9917, https://doi.org/10.1039/c001484b.